

Optimising Graphical Techniques Applied to Irreversible Tracers

Yasser Alzamil^{1,2}, Yulia Hicks¹, Xin Yang¹ and Christopher Marshall³

¹*Institute of Health, Technology and the Digital World, Cardiff University, School of Engineering, Queen's Buildings, The Parade, CF24 3AA, Cardiff, U.K.*

²*Diagnostic Radiology Department, University of Hail, Applied Medical Sciences College, P.O. Box 2440, Hail, Saudi Arabia*

³*Wales Research & Diagnostic Positron Emission Tomography Imaging Centre PETIC, Cardiff University, School of Medicine, UHWM Main Building, Heath Park, CF14 4XN, Cardiff, U.K.*

Keywords: PET, Patlak Graphical Analysis, ¹⁸F-FDOPA Quantification, Image Analysis, Dpetstep Simulation.

Abstract: Graphical analysis techniques are often applied to positron emission tomography (PET) images to estimate physiological parameters. Patlak analysis is primarily used to obtain the rate constant (K_i) that indicates the transfer of a tracer from plasma to the irreversible compartment and ultimately describes how the tracer binds to the targeted tissue. One of the most common issues associated with Patlak analysis is the introduction of statistical noise that affects the slope of the graphical plot and causes bias. In this study, several statistical methods are proposed and applied to PET time activity curves (TACs) for both reversible and irreversible regions that are involved in the equation. A dynamic PET imaging simulator for the Patlak model was used to evaluate the statistical methods employed to reduce the bias introduced in the acquired data.

1 INTRODUCTION

This article describes the first experiment in the optimisation process for ¹⁸F-FDOPA quantification in Parkinson's disease (PD) images. [¹⁸F]FDOPA dynamic images of the brain are used and Patlak graphical analysis will be applied first to the PET data, then several statistical techniques will be implemented to Patlak equations in terms of reducing bias and noise as well as improving the accuracy of the result. The calculation of goodness of fit of the slope and the standard errors of the regression line are the reference for the evaluation of result improvement. Graphical techniques are considered simple for the PET data analysis. Patlak equations for irreversible tracers were used to establish another graphical technique for reversible binding tracers. These techniques are common and preferred due to the independence from compartmental modelling, which is harder compared to the graphical methods. One issue usually generated with this type of analysis is the bias introduced, which is caused by the sensitivity to statistical noise (Logan 2003) that is usually introduced by using the ordinary least squares (OLS) method. This could be reduced by selecting and applying several other methods that

include the feasible generalized linear least squares (FGLS), total least square (TLS), robust fitting regression (RFR).

In this article, these methods first will be applied on simulated phantom PET data generated from dPETSTEP simulation tool (Haggstrom et al. 2016) to see how different statistical methods will affect the image analysis result and how they behave with different levels of noise. The equations, materials, algorithms and tools used in the experiment will be described and the result will be discussed and evaluated in this article.

2 THEORY

The main thing that distinguishes between reversible and irreversible tracers is the experiment length; in other words, a tracer can be reversible over a long period, but it could be irreversible during experiment or scanning time (Logan 2000). For irreversible tracers, the Patlak reference model is used to calculate the [¹⁸F]FDOPA uptake in ROI, and it is the same standard model using the blood data as an input function except that the blood activity is replaced by the activity of a reference TAC. The reference must

be devoid of targeted receptors (Patlak et al. 1983; Patlak and Blasberg 1985). The Patlak method can be modelled as two-tissue compartments (Figure 1).

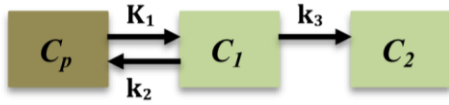


Figure 1: Two-tissue compartmental model where $C_p(t)$ is the plasma tracer concentration at time t . C_1 is the free tracer concentration in tissue and C_2 is the trapped tracer concentration. K_1 , k_2 and k_3 are unidirectional rate constants of the tracer between plasma and tissues.

With FDOPA tracer, the regions used to generate graphics include one reversible region (cerebellum) and one irreversible region (striatum). TACs of blood plasma usually calculated and used an input function for Patlak analysis but a reference tissue region replaces plasma measurement here. Patlak plot equation with reference tissue as an input function, which can be described by

$$\frac{C_{T(t)}}{C_{T'(t)}} = K \frac{\int_0^t C_{T'}(\tau) d\tau}{C_{T'}(t)} + V \quad (1)$$

$$K = \text{slope} = \frac{k_2 k_3}{(k_2 + k_3)} \quad (2)$$

Where $C_T(t)$ is the TAC values of the ROI tissue (striatum), $C_{T'}(t)$ is the reference tissue TAC (cerebellum) at time t , K is the unidirectional net uptake rate constant and V is the blood volume fraction. The equation works for $t > t^*$, t^* is the equilibration time where the radioactivity ratio between reference and ROI tissue becomes reasonably constant (Ikoma et al. 2008). K represents the tracer net uptake calculated from the regression slope, and V is the intercept, which is equal to the volume fraction of blood in ROI tissue at time 0. This means measured activity in ROI (striatum) is divided by the reference tissue activity that represents (y-axis), and plotted against the integral of the reference TAC from the injection time divided by the reference activity, which represents (x-axis). For ^{18}F -FDOPA tracer that targets brain receptors in striatum, the model plot will result in a straight line after t^* (Patlak and Blasberg 1985) as illustrated in (Figure 2).

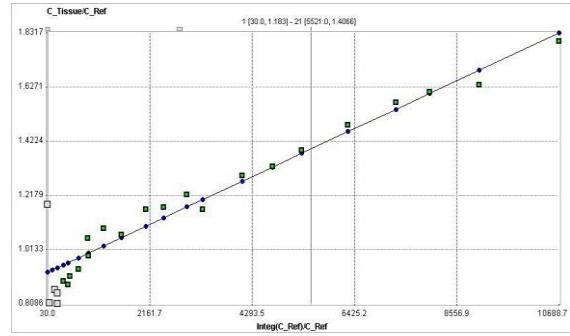


Figure 2: PET activity measured from ROI is divided by the reference tissue activity that represents (y-axis), and plotted against the integral of the reference TAC from the injection time divided by the reference activity, which represents (x-axis). The model plot resulted in a straight line after $t^* = 30$ min in this analysis.

2.1 Ordinary Least Square

OLS is one of the simplest methods of linear regression and it is frequently used to analyse both experimental and observational data. It aims to closely “fit” a function with the data by minimizing the sum of squared differences between the observed responses in the given dataset and those predicted by a linear function. On a plotted graph, this is seen as the sum of the squared vertical distances between each data point in the set and the corresponding point on the regression line (RL). The smaller the differences, the better fitted the model of the data (Hayashi 2000).

In the case of a model with p explanatory variables, the OLS regression model is expressed as:

$$Y = \beta_0 + \sum_{j=1}^p \beta_j X_j + \varepsilon \quad (3)$$

Where Y is the dependent variable, β_0 is the intercept of the model, X_j corresponds to the j^{th} explanatory variable of the model ($j=1$ to p), and ε is the random error with expectation 0 and variance σ^2 . With n observations, the estimation of the predicted value of the dependent variable Y for the i^{th} observation is given by:

$$y_i = \beta_0 + \sum_{j=1}^p \beta_j X_{ij} \quad (4)$$

In a model, this leads to the following estimators of the parameters:

$$\beta = (X^T D X)^{-1} X^T D y \quad \sigma^2 = 1/(W - p^*) \quad (5)$$

$$\sum_{j=1}^n w_i (y_i - y_i)$$

where β is the vector of the estimators of the β_i parameters, X is the matrix of the explanatory variables preceded by a vector of 1s, y is the vector of n observed values of the dependent variable, p^* is the number of explanatory variables to which we add 1 if the intercept is not fixed, w_i is the weight of the i^{th} observation, W is the sum of the w_i weights, and D is a matrix with the w_i weights on its diagonal. The vector of the predicted values can be written as follows (Freedman 2009):

$$y = X (X^T D X)^{-1} X^T D y \quad (6)$$

2.2 Generalized Linear Least Squares

Generalized linear least squares (GLLS) was applied in different PET quantitative model equations (Logan et al. 2001) to remove bias, and it was developed originally by Feng et al. (1993). GLLS is used for estimating the unknown parameters in models based on a linear regression when calculated data shows a certain degree of correlation in the residuals. This method was applied to the data in two parts: for times 0 to T1 and from T1 to the end time. The parameters generated a curve used as input to the linear regression analysis (Logan et al. 2001). The two types of GLLS are called weighted least squares (WLS) and feasible generalized least squares (FGLS). WLS can be applied when all the off-diagonal entries of the covariance error matrix (W) are 0. In FGLS, the opposite occurs when the covariance of errors are unknown (Strutz 2010). With FGLS, the calculation progresses in two steps: first, the residuals are obtained by using OLS to establish the errors covariance matrix that shows a consistency in estimation. Second is implementing the idea of GLLS, which is to divide the data given into two sides, and the part that has the low variance is given more weight than the other sides to generate a more accurate fitted line. With finite samples, an estimator's accuracy with FGLS can be improved by an iteration process where residuals are used to update the errors covariance estimator and consequently FGLS estimation is updated (Long and Trivedi 1992; Freedman 2008; Gujarati 2009). The FGLS estimator may or may not be unbiased in small samples but if (\hat{W}) is a consistent estimator of (W) , then the FGLS estimator is asymptotically unbiased, efficient, and consistent. Monte Carlo studies have shown that the FGLS estimator generally yields better estimates than the OLS estimator (Kennedy 2008).

The general linear regression model is defined by the following set of assumptions:

- Linearity in parameters is the functional form

$$y = X\beta + \mu \quad (7)$$

- Error term has mean zero

$$E(\mu) = 0 \quad (8)$$

- Errors are nonspherical

$$\text{Cov}(\mu) = E(\mu\mu^T) = W \quad (9)$$

Where W is any nonsingular $T \times T$ variance-covariance matrix of disturbances.

- Error term has a normal distribution

$$\mu \sim N$$

- Error term is uncorrelated with each independent variable.

$$\text{Cov}(\mu, X) = 0 \quad (10)$$

There are two types of nonspherical errors: First is when an error term does not have constant variance, and this is called heteroscedasticity. In this type of error, the disturbances are drawn from probability distributions that have different variances and the error term has non-constant variance; the variance-covariance matrix of disturbances is not given by a constant multiplied by the identity matrix (i.e., $W \neq \sigma^2 I$). Second, the errors are correlated, which is called autocorrelation or serial correlation where disturbances are correlated with one another. It occurs when using time-series data. When the disturbances are correlated, the variance-covariance matrix of disturbances is not given by a constant multiplied by the identity matrix (i.e., $W \neq \sigma^2 I$). This is because the elements off the principal diagonal of W , which are the covariance of the disturbances, are non-zero numbers (Granger 1994).

In a general linear regression model stated in matrix format, the sample of T multivariate observations $(Y_t, X_{t1}, X_{t2}, \dots, X_{tk})$ is generated by a process explained below:

$$y = X\beta + \mu, \quad \mu \sim N(0, W) \quad (11)$$

or

$$y \sim N(X\beta, W) \quad (12)$$

An FGLS estimator uses the sample of data to obtain an estimate of W where the true W is replaced with its estimate \hat{W} . The FGLS estimator is given by the rule:

$$\hat{\beta}^{\text{FGLS}} = (X^T \hat{W}^{-1} X)^{-1} X^T \hat{W}^{-1} y \quad (13)$$

The variance-covariance matrix of estimates for the GLS estimator is

$$\text{Cov}(\hat{\beta}) = (X^T \hat{W}^{-1} X)^{-1} \quad (14)$$

The FGLS estimator is also a WLS estimator. The WLS estimated is derived as follows. Find a TxT transformation matrix P such that $\mu^* = P\mu$, where μ^* has variance-covariance matrix $\text{Cov}(\mu^*) = E(\mu^* \mu^{*T}) = \sigma^2 I$. This transforms the original error term μ that is nonspherical into a new error term that is spherical. Use the matrix P to derive a transformed model (Granger 1994; Kennedy 2008):

$$Py = PX\beta + P\mu \quad (15)$$

or

$$y^* = X^* \beta + \mu^* \quad (16)$$

Where $y^* = Py$, $X^* = PX$, and $\mu^* = P\mu$. The FGLS estimator is the OLS estimator applied to the transformed model, which is considered a computational device only to obtain efficient estimates of the parameters and standard errors of the original model of interest.

2.3 Robust Fitting Regression

Robustness denotes the solidity of conclusions and how their differences from assumptions are assigned to a certain model. This means that small changes in the data distribution do not cause large changes in the variance of the estimates (Western 1995). RFR provides an alternative to OLS when assumptions are invalid within the model. RFR provides much improved regression coefficient estimates when data noise or outliers are existent. The influence of outliers is down-weighted by making the outlying residuals larger and simpler to detected, plus performing an iterative procedure to identify outliers and reduce the impact on the coefficient estimates. Robust regression implements its own residual analysis and reduces or completely removes numerous data points, so a decision should be made whether these observations are essential in the analysis (Hintze 2001; Kutner et al. 2004). The most common general method of robust regression is a class of techniques called M-estimators that discount the impact of outlying observations (Fox 2002), introduced by Huber (1964). Consider the linear model

$$y_i = \alpha + \beta_1 x_{i1} + \beta_2 x_{i2} + \dots + \beta_k x_{ik} + \varepsilon_i \quad (17)$$

$$= x_i' \beta + \varepsilon_i$$

The fitted model for the ith of n observations is

$$y_i = a + b_1 x_{i1} + b_2 x_{i2} + \dots + b_k x_{ik} + e_i \quad (18)$$

$$= x_i' b + e_i$$

The general M-estimator minimizes the objective function

$$\sum_{i=1}^n \rho(e_i) = \sum_{i=1}^n \rho(y_i - x_i' b) \quad (19)$$

The function ρ gives the contribution of each residual to the objective function and should have the following properties:

- $\rho(e) \geq 0$
- $\rho(0) = 0$
- $\rho(e) = \rho(-e)$
- $\rho(e_i) \geq \rho(e_i')$ for $|e_i| > |e_i'|$

For least-squares estimation, $\rho(e_i) = e_i^2$, let $\psi = \rho'$ be the derivative of ρ , differentiating the objective function while considering the coefficients b, and assume the partial derivatives to be 0, which enervates a system of k+1 estimating equations for the coefficients:

$$\sum_{i=1}^n \psi(y_i - x_i' b) x_i' = 0 \quad (20)$$

Assume the weight function $w(e) = \psi(e)/e$, and let $w_i = w(e_i)$, then the estimating equations can be written as

$$\sum_{i=1}^n w_i (y_i - x_i' b) x_i' = 0 \quad (21)$$

An iterative solution called iteratively reweighted least-squares (IRLS) is required due to the dependency between weights, residuals and the estimated coefficients. The iteration is performed following these steps:

1. Select initial estimates $b(0)$; for example, the least-squares estimates.
2. At each iteration t, calculate residuals $e_i^{(t-1)}$ and related weights $w_i^{(t-1)} = w[e_i^{(t-1)}]$ from the previous iteration.
3. Apply for new weighted-least-squares estimates

$$b(t) = [X' W^{(t-1)} X]^{-1} X' W^{(t-1)} y \quad (22)$$

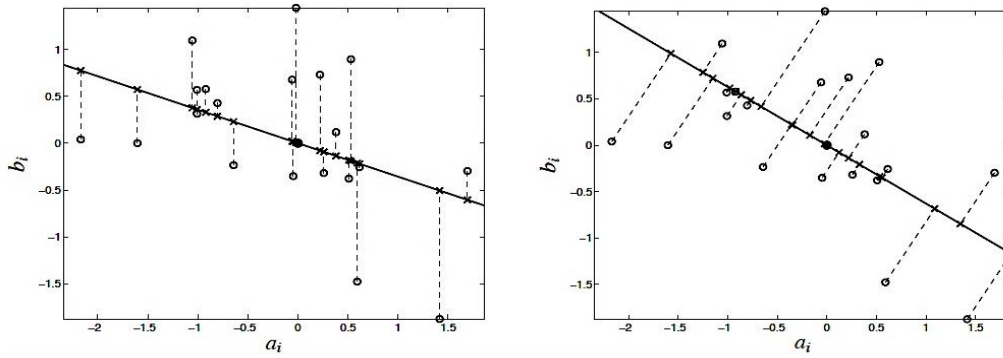


Figure 3: Ordinary least squares (Left) and total least squares (Right) fits of a set of $m = 20$ data points in the plane. (●---) data points, $[a_i \ b_i]$, x- approximations $[\hat{a}_i \ \hat{b}_i]$, solid line (—) fitting model $\hat{a}\hat{x} = \hat{b}$, dashed lines (---) approximation errors.

X is the model matrix, with x_i' as its i^{th} row, and $w_i^{(t-1)} = \text{diag}\{w_i^{(t-1)}\}$ is the current weight matrix. These steps are repeated till the estimated coefficients converge and covariance matrix of b is

$$Vb = \frac{E(\psi^2)}{[E(\psi')]^2} (X'X)^{-1} \quad (23)$$

Using $\sum [\psi(e_i)]^2$ to estimate $E(\psi^2)$ and $[\sum \psi'(e_i)/n]^2$ to estimate $\sum [E\psi']^2$ produces the estimated covariance matrix $\hat{V}(b)$.

2.4 Total Least Squares

The TLS method, known also as error-in-variables method or orthogonal regression method, is a general approach that can be used in n -dimensional space (Petras and Podlubny 2010). Many areas of application use the TLS method such as signal processing, image processing and economics. The orthogonal distance, distance between data point and fitted line, is the main category of TLS and mathematically can be expressed by the following relation (Petráš and Bednářová 2010):

$$R = \sum_{i=1}^n |d_i| \quad (24)$$

d is the orthogonal distance and the target is to find a minimum of R ; the TLS approach minimizes the sum of the squared d from the data points to the fitting line. With the TLS method, well-known mathematical tools are usually used.

For linear regression model of the expression:

$$y = bx + a \quad (25)$$

The coefficients a and b can be derived from the following relations:

$$a = \frac{\sum_{i=1}^n y_i - b \sum_{i=1}^n x_i}{n} = \bar{y} - b\bar{x} \quad (26)$$

$$B = \frac{1}{2} \frac{(\sum_{i=1}^n y_i^2 - n\bar{y}^2) - (\sum_{i=1}^n x_i^2 - n\bar{x}^2)}{n\bar{x}\bar{y} - \sum_{i=1}^n x_i y_i} \quad (27)$$

$$b = -B \pm \sqrt{B^2 + 1} \quad (28)$$

The OLS and TLS methods assess the fitting accuracy in different ways: the OLS method minimizes the sum of the squared vertical distances from the data points to the fitting line, whereas the TLS method minimizes the sum of the squared d from the data points to the fitting line. Figure 3 shows OLS and TLS fitting lines as well as the data approximation. In the least squares case, the data approximation is obtained by correcting the second coordinate only. In TLS, the data approximation is obtained by correcting both coordinates (Markovsky and Van Huffel 2007). This method takes into account the noise in the independent as well as dependent variables (Varga and Szabo 2002).

3 MATERIALS AND METHODS

3.1 Scanner and Reconstruction Parameters

The scanner available in the PET Imaging Centre at the University Hospital of Wales is GE Discovery 690 PET/CT (General Electric Healthcare), and it is made for clinical and research use. The reconstruction method used with FDOPA imaging is a maximum likelihood ordered subset estimation maximisation (ML OSEM) with Vue Point FX algorithm with time of flight (TOF) correction.

3.2 dPETSTEP and Simulation Parameters

dPETSTEP is a dynamic PET simulator that can generate PET brain images and allows full simulation of kinetic modelling (Haggstrom et al. 2016). Additionally, the dynamic PET data can then be model-fitted to produce physiological parameter estimates. dPETSTEP uses MATLAB as a platform and works as an extension of another application named PETSTEP, and they both share some commands. Both applications are open source and available on the GitHub© website. dPETSTEP is a fast and simple tool and can be used as an alternative to Monte Carlo (MC), as it is 8000 times faster than MC. In terms of kinetic analysis, dPETSTEP is very helpful for the evaluation of different processing choices with dynamic and parametric images that usually require a long time for image analysis where each pixel is analysed. To run the simulation, at the beginning, the settings of the simulation must be adjusted to be consistent with the PET scanner features that are targeted by the analysis or evaluation. Table 1 shows all required simulation settings to generate simulated dynamic PET data for ^{18}F -FDOPA images that are performed for a PD patient. The simulated dynamic PET scan will be acquired as 26 time frames over 94.5 min (1×30 sec, 4×1 min, 3×2 min, 3×3 min, and 15×5 min) with a dose of 111 MBq. The cerebellum region from each time frame will be used as the reference region tissue (input function) for the quantitative analysis. The output after running the simulator is a 4D matrix with a reconstructed dynamic ordered subset expectation maximization (OSEM) image with point spread function (PSF) correction, which is similar in features to the dynamic PET data produced by the real scanner. The noise level of the 4D matrix is kept at a minimum in its sinogram. The entire volume of images is separated into single slices as 2D images (Figure 4), and these are saved to a MATLAB version 4 MAT-file, which allows them to be loaded in any MATLAB version with 2D double, character, sparse arrays and without compression. This version allows for each variable to have a maximum size of 100 million elements per array and 231 bytes per variable, which allows all the data information to be kept without losing any details. Scatter and decay correction was applied during the reconstruction process obtained from setting the parameters file within the simulation codes. All slices introduced by the 4D matrix are exported to PMOD 3.4 software to perform further analysis in kinetic modelling with specific ROI.

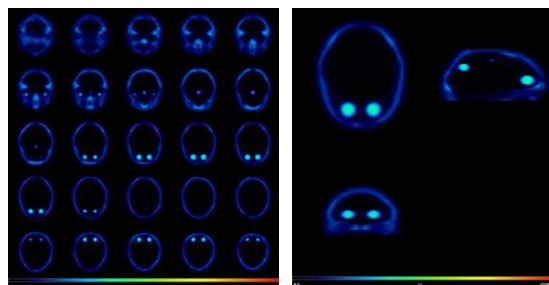


Figure 4: (Left) The entire volume of images is separated into single slices as 2D images, which are saved to a MATLAB version 4 MAT-file, which allows them to be loaded to PMOD software (Right).

3.3 PMOD Software

PMOD software has been designed for researchers in the molecular imaging field and provides suitable tools for all quantitative data processing steps. This will make researchers pay more attention to the content and clinical data rather than programming new tools from scratch. PMOD can process all type of images such, as CT, MR and SPECT, in many different imaging formats, from simple processing tasks to sophisticated protocols and analysis all packed into one graphical user interface application. It is validated and refers to more than 1000 peer-reviewed publication documents on kinetic modelling and biomedical research (LLC 2017). In this experiment, two applications are used for the analysis, PBAS and PKIN, which allow import of the simulated dynamic PET images and applying kinetic analysis, respectively. PBAS is the main tool in PMOD and can receive images in different proper formats, one of which is v4 MAT-files, which should be imported to PBAS as double SE data form. The images imported must be in Bq/cc units, and the orientation should be corrected if it looks different. All corrections are already made by the simulator, and PMOD should do nothing in terms of corrections. At the beginning, all slices are merged into frames again, and the times for each frame are consistent with the protocol used with the simulator. After that, all frames are saved as DICOM format, the Digital Imaging and Communications in Medicine standard. This format is data rich, and the header information includes attenuation, scatter and decay correction, normalisation, frame timing and reconstruction parameters as well as the standard, required details of matrix dimensions and pixel size. The computer which was used for reconstruction of the images was an Intel® Core™ I7-6700K processor 8MB Cache 4.00 GHz 4 Cores 8, with Windows 7 Enterprise 64-bit OS and 32 GB RAM.

PBAS was used to draw and analyse the ROI (left striatum) and reference tissue (cerebellum), the reason for choosing the left striatum is that it is assumed that in simulated images both the left and right side will have the same amount of radioactivity. The net influx rate constant (K_i) is usually calculated over a range of 30-90 min for dynamic images, so all frames between 30 and 90 minutes are averaged into slices, and then the ROIs are drawn on all slices to show them. Two volumes of interest (VOIs) at minimum must be created; one VOI for the cerebellum represents the reversible region, and another one for the left striatum represents the irreversible region. For regional analysis, the ROI is drawn as one complete contour; ROI objects were drawn freehand (Figure 5).

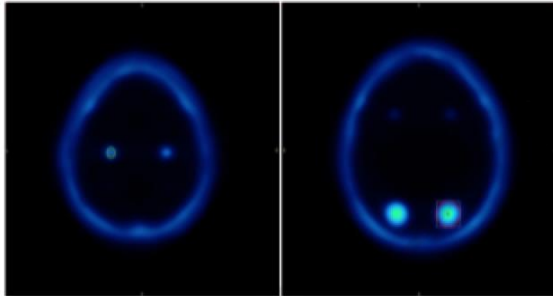


Figure 5: For regional analysis, the ROI is drawn as one complete contour; ROI objects were drawn freehand; simulated striatum (Left) and part of simulated cerebellum (Right).

Each VOI includes contours that are drawn over the simulated anatomical region required for the analysis, and all VOIs are saved in a single file to be used again as a template. In fact, even the ROIs' contours are drawn on the averaged dynamic frames; however, the TACs at the end will be obtained from the original dynamic PET volume. So, the images are averaged to help guiding the drawing on all slices that show ROIs. Then, the time activity curves (TACs) are generated from the contours of regions required for the analysis. TACs for all regions must be checked, and the tracer in the reversible curve should show a clear washout. PMOD has an algorithm to determine the best time for t^* . In this experiment, the Patlak reference tissue analysis is based on $t^* = 30$ min, and this is important for slope calculations (K_i value). For regional analysis, the result will be (K_i) value (slope). For each specific ROI made, the intercepts that represent (V), standard errors (SE) and Chi-square are calculated within the analysis. The maximum standard error accepted for (K_i) is 10%.

The simulation of the FDOPA dynamic PET data is repeated 10 times and simulates different (K_i) values within the normal healthy subjects, which are between 0.012 and 0.014 according to literature, considering that the imaging protocol of FDOPA for scanning patients is based on giving both carbidopa and entacapone. After finishing the kinetic modelling analysis, Gaussian noise with a zero mean was applied in 10 levels (0.05 – 0.5) for both the reference tissue and ROI. All the TACs were then exported to be analysed by our statistical calculation methods, FGLS, TLS and RFR, which were explained before. Codes were written in MATLAB software to analyse all TACs obtained from the simulated images processed by PMOD, and the (K_i) results were saved to Excel sheets. The following section illustrates the results for the simulated data, including statistics, which were calculated to evaluate how the methods affected the estimate of the final (K_i) values.

4 RESULTS

TACs for reference tissue (cerebellum) and ROI (left striatum) that were obtained from the first simulation data without noise are plotted as an example in Figure 6. The curves show that activity in the cerebellum starts to increase significantly, reaching 12000 Kbc/cc, and then decreases (washout) to around 4000 Kbc/cc and starts what is known as the equilibration stage, which is the time point most preferable for Patlak analysis. The activity washout confirms the reversibility of the cerebellum region. In contrast, the left striatum TAC increased until it reached a stable level for the remainder of the scan, which confirms the irreversibility. For OLS, FGLS, TLS and RFR calculation, the results include noisy and non-noisy data. After fitting the data in the statistical models, two numerical methods used to evaluate the goodness of fit for all linear regression analyses were included: the sum of squares due to error (SSE) and the standard error (SE), known as the root mean squared error (RMSE) as well. The numerical measures are more closely concentrated on a specific aspect of the data and often try to compress that information into a single number. SSE measures the total deviation of the response values from the fit, where a value closer to 0 indicates a smaller random error component within the model selected, and the fit will be more useful for prediction. It is also known as the summed square of residuals.

$$SSE = \sum_{i=1}^n (y_i - \hat{y}_i)^2 \quad (29)$$

Where y_i is the i^{th} value of the variable to be predicted, \hat{y}_i is the predicted value of y_i . SE is an estimate of the standard deviation of the random components in the data and is similar to the SSE. An SE value closer to 0 indicates a fit that is more useful for estimation. SE is described as

$$SE = \sqrt{MSE}, MSE = \frac{SSE}{v}, v = n - m \quad (30)$$

Where MSE is the mean square error or the residual mean square and v indicates the number of independent pieces of information involving the n data points that are required to calculate the sum of squares, which is calculated as the number of response values n minus the number of fitted coefficients m estimated from the response values.

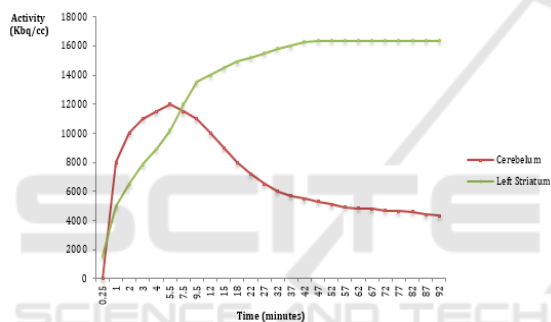


Figure 6: TACs for the reference tissue (cerebellum) and ROI (left striatum) that were obtained from the first simulation data without noise are plotted as an example.

A one-way repeated measured analysis of variance (ANOVA) was conducted to evaluate the null hypothesis that there is no change in the simulations' Ki value when calculated with different statistical regression models in all four groups ($N = 10$). The results of the ANOVA indicated a significant effect, Wilks' Lambda = .001, $F(3, 7) = 41.17$, $p < 0.01$, $\eta^2 = .75$. Thus, there is significant evidence to reject the null hypothesis. Follow-up comparisons indicated that each pairwise difference was significant, $p < 0.01$, except between OLS and TLS, where $p = 0.09$. There was a significant difference between the statistical models used, suggesting that using a different linear regression model reveals a different Ki value, which is the main parameter of diagnosis. A repeated measures ANOVA is performed when the samples are considered related (dependent) and more than two groups. Table 2 illustrates the SE and SSE for each method applied to simulation data. With the

OLS method, the min SE in all simulations including noisy data was 0.05680 and the max was 1.01070; the average SE was 0.23551. For SSE, the min was 0.00029, max 0.09286 and the average 0.00741. The fold change range was between 0.00041 and 2.09565. FGLS calculations with the data showed the SE min was 0.0012377, max 0.0105768 and the average 0.0041978. The SSE min was 0.0000001, max 0.0000102 and the average 0.0000020, with a general fold change range of 0.0032366-2.3815366. For TLS analysis, the min SE was 0.05337, max 18.79341 and the average SE in all data calculations was 2.86733. The SSE min was 0.00026, max 32.10839 and average 1.58100. The fold change range was 0.00506-2.09567. The min SE in the RFR analysis was 0.07026, max 0.92162 and the average 0.37945. The SSE min was 0.00045, max 0.07722 and the average 0.01797 with a fold change range of 0.00755-2.83829.

Table 1: A one-way repeated measured analysis of variance (ANOVA) result.

Test	Wilks' Lambda	F(3, 7)	p-value
ANOVA (N=10)	.001	41.17	$p < 0.01$
	pairwise difference	OLS and TLS, pairwise	η^2
	$p < 0.01$	$p = 0.09$.75

Table 2: SE and SSE values for each method applied to simulation data.

Stat. Model		SE	SSE	fold change
OLS	Min	0.0568	0.0003	0.0003
	Max	1.0107	0.0929	-
	Avg.	0.2355	0.0074	0.7927
FGLS	Min	0.0012	0.1×10^{-6}	0.0049
	Max	0.0106	10.2×10^{-6}	-
	Avg.	0.0042	2.0×10^{-6}	2.5119
TLS	Min	0.0697	0.0004	0.0107
	Max	1.3071	0.1553	-
	Avg.	0.4505	0.0237	2.0719
RFR	Min	0.0703	0.0005	0.0196
	Max	0.9216	0.0772	-
	Avg.	0.3795	0.0180	1.6780

5 DISCUSSION

For most of the Ki values, it increases in proportion to the level of noise. SE and SSE also increase with higher noise level. In simulations 1-5, the data behaved quite similarly with the noise effect compared to simulations 6-10, which had more scattering, and this could have been caused by

increasing the K_i amount for the data without noise. A one-way repeated measurements ANOVA test indicated that there is significant evidence to reject the null hypothesis and confirm that those statistical models reveal different results for the final K_i value. Each statistical regression model dealt with the simulation data in a different way, and based on the goodness of fit evaluations, the best fitted regression model can be chosen. Follow-up comparisons indicated that each pairwise difference was significant except between OLS and TLS. The p -value between OLS and TLS shows that null-hypothesis about equality can not be rejected at confidence level 0.05 that is used with this test. The significant difference between the statistical models used, suggesting that using a different linear regression model reveals a different K_i value, which is the main parameter of Parkinson's disease diagnosis. The min SE and SSE were found with FGLS, and this suggests that FGLS is the best of these models to fit the noisy data. FGLS also had the second lowest fold change rate, which measures the change difference from the K_i value without noise. OLS and TLS showed the lowest fold change rate, and that indicates more resistance to the noise effect than the other methods. RFR had the highest fold change rate compared to the data without noise, which indicates sensitivity to noise.

In the first simulation, the OLS K_i data had similar values at all levels of noise, unlike the other data for the rest of the simulations. For the first two simulations, all statistical regression models behaved similarly at all noise levels; thus, the K_i data points were close in value. This could happen in link to the original K_i values without noise where considered the lowest among the other simulations. Other simulations with low K_i values below 0.012, which represents the diseased levels, could reveal more details about how statistical models will behave. In addition, K_i values lower than 0.012 could clarify whether the noise could lead to moving the K_i values to be considered normal. The big difference within the SE from one noise level to another indicates the high sensitivity to noise in linear regression analysis, which confirms the previous results in the published literature review. The experiment has contributed to the knowledge in the field by suggesting using FGLS as a linear regression method for Patlak graphical analysis. From the above results, using FGLS could provide better data fitting with low SE and SEE, indicating more accurate results than other approaches. Including lower K_i values without noise could give more details and better confirms the best fitting model from regression methods. Repeating the

experiment with different equivalent time (t^*) points could reveal more details and alter the accuracy of those methods. It would be useful to apply those models on clinical data obtained from patient dynamic images and compare the results to the outcome of this experiment.

6 CONCLUSION

Graphical techniques in PET data analysis from reference tissue are considered simple means of analysis to obtain physiological parameters. One issue usually generated with this type of analysis is the bias introduced, which is caused by the sensitivity to statistical noise. The study shows there is a significant difference between the statistical models used, suggesting that using a different linear regression model reveals a different K_i value, which is the main parameter of Parkinson's disease diagnosis. Analysing the PET data with different statistical regression approaches and evaluating each approach graphically and numerically could improve the final result for more accurate diagnosis. FGLS regression model could provide better data fitting in Patlak analysis with low SE and SEE, indicating more accurate results than other approaches. In the next work, these methods will be applied to clinical PET data obtained from a clinical trial to see how the final result will be affected.

REFERENCES

- Feng, D., Wang, Z. and Huang, S.-C. 1993. A study on statistically reliable and computationally efficient algorithms for generating local cerebral blood flow parametric images with positron emission tomography. *Medical Imaging, IEEE Transactions on* 12(2), pp. 182-188.
- Feng, D. et al. 1996. An unbiased parametric imaging algorithm for nonuniformly sampled biomedical system parameter estimation. *Medical Imaging, IEEE Transactions on* 15(4), pp. 512-518.
- Fox, J. 2002. Robust regression. An R and S-Plus companion to applied regression.
- Freedman, D. A. 2008. On regression adjustments to experimental data. *Advances in Applied Mathematics* 40(2), pp. 180-193.
- Freedman, D. 2009. *Statistical models: theory and practice*. Cambridge: Cambridge University Press.
- Granger, C. W. J. 1994. Learning and practicing econometrics: Griffiths, We, Hill, Rc, Judge, Gc. *Journal of Economic Literature* 32(1), pp. 115-122.
- Gujarati, D. N. 2009. *Basic econometrics*. Location: Tata McGraw-Hill Education.

- Haggstrom, I., Beattie, B. J. and Schmidlein, C. R. 2016. Dynamic PET simulator via tomographic emission projection for kinetic modeling and parametric image studies. *Med Phys* 43(6), p. 3104.
- Haggstrom, I. et al. 2016. A fast dynamic PET simulator for improved kinetic modeling estimation. *Journal of Nuclear Medicine* 57(supplement 2), pp. 477-477.
- Hayashi, F. 2000. *Econometrics*. Princeton, New Jersey: Princeton University Press.
- Hintze, J. 2001. NCSS and Pass. Number Cruncher Statistical Systems, Kaysville.
- Huber, P. J. 1964. Robust estimation of a location parameter. *The Annals of Mathematical Statistics* 35(1), pp. 73-101.
- Ikoma, Y. et al. 2008. PET kinetic analysis: error consideration of quantitative analysis in dynamic studies. *Annals of Nuclear Medicine* 22(1), pp. 1-11.
- Kennedy, P. 2008. *A guide to econometrics*. 6th ed. Malden, Massachusetts: Blackwell Pub.
- Kutner, M. H., Nachtsheim, C. and Neter, J. 2004. *Applied linear regression models*. Location: McGraw-Hill/Irwin.
- LLC, P. T. 2017. PMOD Biomedical Image Quantification. [Format type]. Available at: http://www.pmod.com/web/?page_id=476 [Accessed: date].
- Logan, J. 2000. Graphical analysis of PET data applied to reversible and irreversible tracers. *Nuclear Medicine and Biology* 27(7), pp. 661-670.
- Logan, J. 2003. A review of graphical methods for tracer studies and strategies to reduce bias. *Nuclear Medicine and Biology* 30(8), pp. 833-844.
- Logan, J. et al. 2001. A strategy for removing the bias in the graphical analysis method. *J Cereb Blood Flow Metab* 21(3), pp. 307-320.
- Long, J. S. and Trivedi, P. K. 1992. Some specification tests for the linear regression model. *Sociological Methods & Research* 21(2), pp. 161-204.
- Markovskiy, I. and Van Huffel, S. 2007. Overview of total least-squares methods. *Signal Processing* 87(10), pp. 2283-2302.
- Patlak, C. S. and Blasberg, R. G. 1985. Graphical evaluation of blood-to-brain transfer constants from multiple-time uptake data: generalizations. *J Cereb Blood Flow Metab* 5(4), pp. 584-590.
- Patlak, C. S., Blasberg, R. G. and Fenstermacher, J. D. 1983. Graphical evaluation of blood-to-brain transfer constants from multiple-time uptake data. *J Cereb Blood Flow Metab* 3(1), pp. 1-7.
- Petráš, I. and Bednárová, D. 2010. Total least squares approach to modeling: a MATLAB toolbox. *Acta Montanistica Slovaca* 15(2), p. 158.
- Petras, I. and Podlubny, I. 2010. Least Squares or Least Circles? A comparison of classical regression and orthogonal regression. *Chance* 23(2), pp. 38-42.
- Strutz, T. 2010. *Data fitting and uncertainty: a practical introduction to weighted least squares and beyond*. Location: Vieweg and Teubner.
- Varga, J. and Szabo, Z. 2002. Modified regression model for the Logan plot. *Journal of Cerebral Blood Flow & Metabolism* 22(2), pp. 240-244.
- Western, B. 1995. Concepts and suggestions for robust regression analysis. *American Journal of Political Science* 39(3), pp. 786-817.